



## Fault reactivation and selective abandonment in the oceanic lithosphere

M. Delescluse,<sup>1,2</sup> L. G. J. Montési,<sup>3</sup> and N. Chamot-Rooke<sup>1</sup>

Received 20 June 2008; revised 21 July 2008; accepted 24 July 2008; published 29 August 2008.

[1] Normal and transform faults originally formed at a spreading-centre can be reactivated in diffuse plate boundary zones and in areas of lithospheric flexure such as at peripheral bulges to subduction zones. Using new seismic reflection profiles and modeling, we investigate how the original oceanic fabric is reactivated in the simple case of fault perpendicular compression. In the Central Indian Basin, well-oriented normal paleofaults were reactivated with reverse motion at the very onset of deformation (9 Ma) but only a small subset remained active past  $\sim 7$  Ma, suggesting that most of the densely spaced small-offset faults were abandoned while deformation localized onto fewer faults with larger spacing. We find a similar evolution using a 2D finite element code of lithospheric shortening using a pseudoplastic rheology. Weak zones, 3 km-spaced and 30–40% weaker than the surrounding material, are introduced to simulate the fabric formed at the ridge axis. We show that reactivation and selective abandonment require strain weakening followed by strain-rate weakening once a maturation threshold is reached. A maturation fault slip of less than 50 m is needed to produce a fault network similar to that in the Central Indian Ocean. **Citation:** Delescluse, M., L. G. J. Montési, and N. Chamot-Rooke (2008), Fault reactivation and selective abandonment in the oceanic lithosphere, *Geophys. Res. Lett.*, 35, L16312, doi:10.1029/2008GL035066.

### 1. Introduction

[2] The rigidity of the oceanic in comparison to the continental lithosphere means that there is relatively little deformation away from plate boundary zones. However, the oceanic lithosphere does deform when highly stressed [e.g., Okal, 1983; Gordon, 2000], and these rare intraplate deformation areas constitute excellent natural laboratories to investigate faulting processes. Among these, the Indian Ocean presents undoubtedly the best active example [Eittreim and Ewing, 1972; Weissel *et al.*, 1980; Bull and Scrutton, 1992; Chamot-Rooke *et al.*, 1993; Krishna *et al.*, 2001]. The India-Australia oceanic plate is actively deforming in a wide equatorial region running from the Central Indian ridge to the west to the Sumatra Trench to the east, with a great variety of stress orientations and styles of faulting [Cloetingh

and Wortel, 1986; Tinnon *et al.*, 1995; Delescluse and Chamot-Rooke, 2007]. Several areas (A to D in Figure 1) contain ubiquitous evidence for fault reactivation, as described next, working from west to east.

[3] 1. A large earthquake (Mw 7.6) ruptured a fossil portion of a transform fault at short distance from the Carlsberg Ridge (A in Figure 1) [Bohnenstiehl *et al.*, 2004]. The sense of slip and the localization of the after-shocks were interpreted as resulting from diffuse intraplate extension [Antolik *et al.*, 2006].

[4] 2. The Central Indian Basin (CIB) (B) is widely affected by inversion. Weissel *et al.* [1980] pointed out that fracturing was occurring not on shallow-angle thrusts faults, but on high-angle faults further interpreted as reactivation of pre-existing faults originally formed at the spreading axis [Bull and Scrutton, 1990; Montési and Zuber, 2003a] (Figure 2). Statistics on faults imaged within the crust down to Moho depth [Bull and Scrutton, 1992; Chamot-Rooke *et al.*, 1993] show that most angles are indeed steep (about  $4^\circ$ ), the original normal fault being reactivated (Figure 2a).

[5] 3. In the eastern CIB and in the Wharton Basin (C), N–S fracture zones are reactivated with a sinistral strike-slip motion decoupling the Australia plate from its Indian counterpart [Deplus *et al.*, 1998; Delescluse and Chamot-Rooke, 2007]. The same network of sinistral faults was reactivated immediately after the great Sumatra earthquake.

[6] 4. The foretrench bulge offshore Sumatra displays active normal faults related to bending. Most of these are neoformed faults (D in Figure 1) since the original fabric is severely misoriented in the Wharton Basin with respect to the flexural stresses as observed and modelled elsewhere [Masson, 1991; Ranero *et al.*, 2003; Billen *et al.*, 2007]. However, a few focal mechanisms indicate slip onto the original E–W faults in the region where the fossil Wharton ridge meets the trench (D').

[7] In summary, the oceanic fabric of the Indian Ocean lithosphere from the Carlsberg Ridge to the Sumatra Trench is presently reactivated in a variety of tectonic settings. Intriguingly, this fabric is never totally reactivated. Instead, deformation is localized onto a selection of faults from the original network. The history of reactivation is clearest in the Central Indian Ocean where the lithosphere was formed at spreading-centres with short segment lengths at Cretaceous to Eocene time. There, the sedimentation of the Bengal Fan acts to record the evolution of deformation through time with high fidelity, and seismic reflection imaging can be used to unravel this history.

### 2. Selective Abandonment of Faults in the CIB

[8] Figure 2 presents portions of one multichannel line (Phèdre Leg 1 survey [Chamot-Rooke *et al.*, 1993]), and

<sup>1</sup>Laboratoire de Géologie, Ecole Normale Supérieure, CNRS, Paris, France.

<sup>2</sup>Paris XI University, Orsay, France.

<sup>3</sup>Department of Geology, University of Maryland, College Park, Maryland, USA.

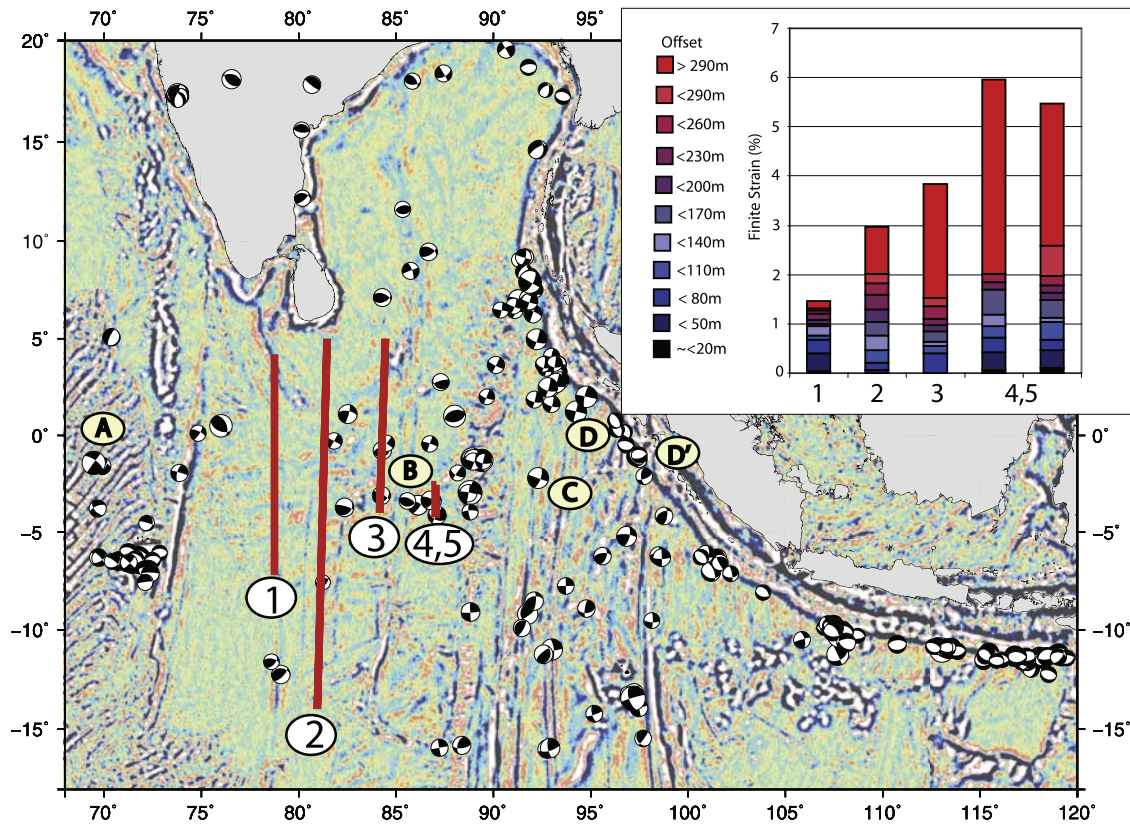


**Figure 1.** Style of deformation in the northeastern Indian Ocean. Background is a Sandwell 15.1 satellite free-air gravity [Sandwell and Smith, 1997], filtered to enhance the oceanic fabric. Areas A to D are discussed in the introduction. Focal mechanisms are from the Harvard CMT catalog (1976–2008), older historical mechanisms are those compiled by Delescluse and Chamot-Rooke [2007]. Four seismic tracks are displayed: (1) Conrad, (2) Phèdre Leg 1, (3) Phèdre Leg 2, (4) & (5) Andaman P102 & P103. Inset is the observed finite strain (in %) for each profile discretized into several fault-offset ranges.

two high resolution seismic profiles acquired during the Andaman 2000 survey (see Figure 1 for their location). Figure 2a clearly shows an inverted basin: the original normal fault, traced inside the crust, is presently reused as thrust. Reverse motion on this fault is kilometric, and many others large-offset faults have been imaged through seismic profiling [Bull and Scrutton, 1992; Chamot-Rooke et al., 1993; Van Orman et al., 1995]. Small-offset faults have received less attention: they require high resolution seismic surveys to be imaged, and they are inferred to contribute little to the total shortening [Van Orman et al., 1995]. Figures 2b and 2c show that these small-offset reverse faults are frequent. Their mean spacing (3 km) matches the expected initial normal faults spacing, suggesting that they do represent the original fabric acquired at the ridge axis. This spacing is significantly less than the 5–11 km reported earlier [Chamot-Rooke et al., 1993; Van Orman et al., 1995] due to the incompleteness of the fault catalogues towards the small offsets.

[9] Careful re-examination of the seismic lines shows that deformation started prior to the main Upper Miocene unconformity drilled at ODP Leg 116 site: the onset of significant deformation is around 7 Ma [Cochran et al., 1989], but faults were active as early as 9 Ma [Delescluse and Chamot-Rooke, 2008], and even possibly earlier but at smaller strain rate (K. S. Krishna et al., Early (pre-8 Ma

fault activity and temporal strain accumulation in the central Indian Ocean, submitted to *Geology*, 2008). In detail, Figure 2d shows that even after flattening of the 7 Ma unconformity, the earlier 9 Ma presents reverse offsets at small faults that nucleate in the basement. These small-offset faults become inactive soon after the onset of deformation, as the thick sedimentary sequence above the 7 Ma unconformity remained undeformed. High resolution profiler data confirmed that many of these small faults have no present-day surface expression which means that only a widely-spaced subset of these faults remain active to the present. Today, tilted blocks bounded by the largest faults have a longer 20–30 km spacing. Notice that some of these major faults localized deformation from the very onset throughout (Figure 2).

[10] We performed a systematic binning of the cumulative fault slip along seismic lines that cross the deformation zone in order to quantify shortening accommodated by different fault-offset ranges (Figure 1). As previously discussed by a number of authors, the total amount of shortening is increasing from west to east as a result of India-Australia kinematics [DeMets et al., 2005]. However, faults with small offsets do not follow this eastward increase: they accommodate the same amount of shortening (~1%) in the west (where they accommodate most of the deformation) and in the east (where they accommodate only a small



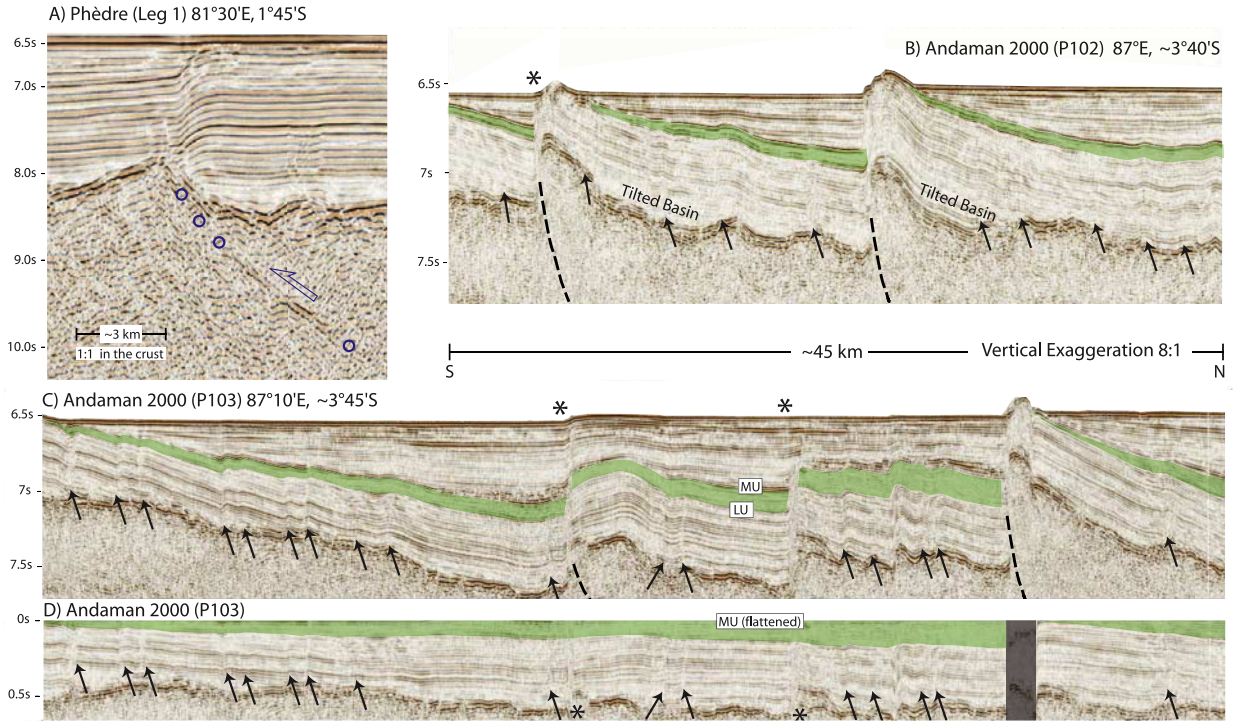


**Figure 2.** (a) Multichannel line (Phèdre Leg 1 survey) showing an inverted basin and associated reverse fault in the crust (1:1). (b) High resolution P102 profile shows typical tilted blocks bounded by the main active faults and inactive small offset faults (black arrows). The green layer shows a syn-tectonic sequence below the main unconformity (MU, ~7 Ma) and above the lower unconformity (LU, ~9 Ma). (c) P103 profile. (d) Same profile but with the MU unconformity flattened to better visualize prior deformation. Notice the pre-7 Ma deformation (black arrows). Stars in B and C pinpoint areas where the main reverse fault nucleates on the side of a pre-existing horst structure but with “wrong” vergence (i.e. neoformed fault dipping opposite to the preexisting fault), suggesting that heterogeneities rather than the fault itself act as the main trigger.

part of deformation). Note that small offset faults are not resolved in the Phèdre lines as only low frequency seismic data are available.

[11] Based on the observations, we hypothesize the existence of a threshold process whereby most reactivated faults are abandoned after a given amount of slip. Deformation then concentrates on fewer still active larger faults. We call this process selective abandonment.

### 3. Modeling Strain and Strain-Rate Weakening With LAYER

[12] We model the selective abandonment of reactivated faults using the Lagrangian finite element code LAYER [Neumann and Zuber, 1995]. This software utilizes a viscous-pseudoplastic rheology [Chen and Morgan, 1990], whereby the viscosity in each element,  $\eta$ , is adjusted from a value consistent with power law creep,  $\eta_{pl}$  to limit strain to a yield strength  $\sigma_y$

$$\eta = \min\left(\eta_{pl}, \sigma_y / 2\dot{\epsilon}_{II}\right) \quad (1)$$

where  $\dot{\epsilon}_{II}$  is the second invariant of the strain rate in each element.

[13] Neumann and Zuber [1995] implemented a strain-rate weakening law to simulate the localization of deforma-

tion along narrow zones (faults) in a pseudo-brittle over ductile two-layer medium in extension [Neumann and Zuber, 1995; Behn et al., 2002] and in compression [Montési and Zuber, 2003b]. In these studies, faults initiate based on numerical noise rather than a priori constraints. However, a fault network with systematic fault spacing develops simultaneously to longer wavelength lithospheric buckling [Montési and Zuber, 2003c].

[14] At variance with Montési and Zuber [2003a], who suggested reactivation only in the vicinity of predicted localization instability wavelength, our new data lead us to consider the near complete reactivation of the spreading ridge normal faults. To capture this behavior, we modified LAYER to consider both strain weakening and strain-rate weakening (Figure 3). The yield strength increases with depth according to

$$\sigma_y = (C_0 + C\rho gz)K \quad (2)$$

where  $C_0$  is the cohesion,  $C$  the frictional term,  $\rho$  the density,  $g$  the acceleration of gravity, and  $K$  is the weakening factor. There are two sources of weakening. Initially, the yield strength decreases linearly with strain, by a factor  $W_s$ , up to a critical strain  $\epsilon_s$ . When strain exceeds a maturation threshold  $\epsilon_m$  (equivalent to a critical fault slip), the weakening factor becomes strain-rate dependent [Marone and Cox, 1994; Beeler et al., 1996].

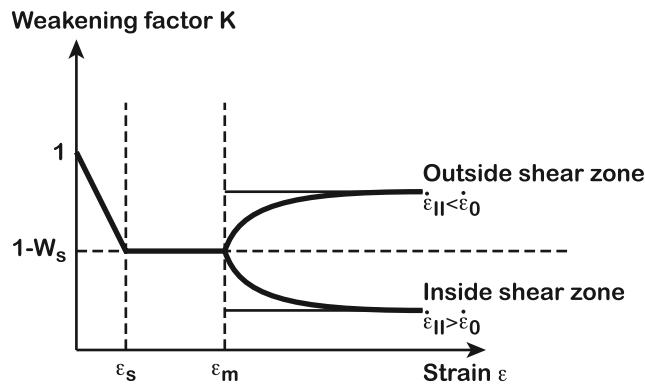


**Figure 3.** Evolution of the weakening factor with strain. For strain less than  $\varepsilon_s$ , strength weakens with strain but beyond a maturation threshold  $\varepsilon_m$ , strength depends on strain rate. Strength is reduced in shear zones, where strain rate is high (thin line, instantaneous change in strain rate; thick line, progressive change) and vice-versa between shear zones.

[15] The complete expression of  $K$  is as follows

$$K = \begin{cases} 1 - W_s(\varepsilon/\varepsilon_s) & \varepsilon < \varepsilon_s \\ 1 - W_s & \varepsilon_s < \varepsilon < \varepsilon_m \\ (1 - W_s)[1 - W_r \log(\dot{\varepsilon}_{II}/\dot{\varepsilon}_0)] & \varepsilon > \varepsilon_m \end{cases} \quad (3)$$

where  $\dot{\varepsilon}_0$  and  $W_r$  are normalization values (parameter values in auxiliary material Table S1<sup>1</sup>).

[16] The preexisting fabric is represented by patches with non-zero initial strain dipping uniformly and spaced every 3 km (see auxiliary material Text S1 and Figure S1). These weak patches are equivalent to the reduced friction necessary to reactivate slightly oblique preexisting normal faults at trenches [Billen *et al.*, 2007]. The entire model is 225 km long and 80 km thick, with  $900 \times 160$  elements. Element height increases progressively with depth. The modeled lithosphere is shortened at a constant rate with time ( $\sim 6.3 \times 10^{-9} \text{ yr}^{-1}$ ).

[17] A model that best resembles the central Indian Ocean fault network is shown in Figure 4. Initially, the network of initial strain patches is reactivated uniformly so that after 1.8 Ma of shortening (top), all the initial faults display a small displacement. Subsequently, only a few of the reactivated faults accumulates significant displacement, leading to a network of major faults and pop-up structures with a spacing that is consistent with the localization instability of Montési and Zuber [2003c]. A wide variety of models were run to test the sensitivity to the model parameters. Timing of the transition from reactivation to selection is mainly controlled by the maturation threshold. A  $\sim 2$  Myr maturation time, as we document in the CIB, requires a maturation slip of less than 50 m. This short period is similar to the stress build-up time required to form the long wavelength lithospheric buckling in previous modeling [Gerbault, 2000]. A longer maturation period is possible in the model, but it would require very slow deformation rate in the early stage to keep the contribution of the small faults around 1%

of the total strain, as observed. After 9 Myr of shortening (middle), only major faults are active. Nevertheless, the initial fault network has accumulated sufficient strain (about 1.1% of the total shortening, bottom) to produce structures visible in high resolution seismic data.

#### 4. Conclusions

[18] Our new data point to an early onset of significant deformation in the Central Indian Ocean around 9 Ma. At that time, the entire fault network formed at the ridge axis was reactivated. Few of these faults remained active beyond the time of the major Upper Miocene unconformity (around 7 Ma) following a selective abandonment process. Our modeling offers a physical mechanism for such a process. Strain weakening controls the localization of deformation in the early stage, until strain-rate weakening becomes dominant. The remaining major active faults bound blocks that are 20 to 30 km spaced in the model, with regularly-spaced internal faulting within the blocks themselves. Seismic lines show tilted blocks of the same size bounded by major faults with hundreds of meters of cumulated slip. The maximum offset of the finely spaced fault set constrains the critical offset over which strain weakening is active to be less than

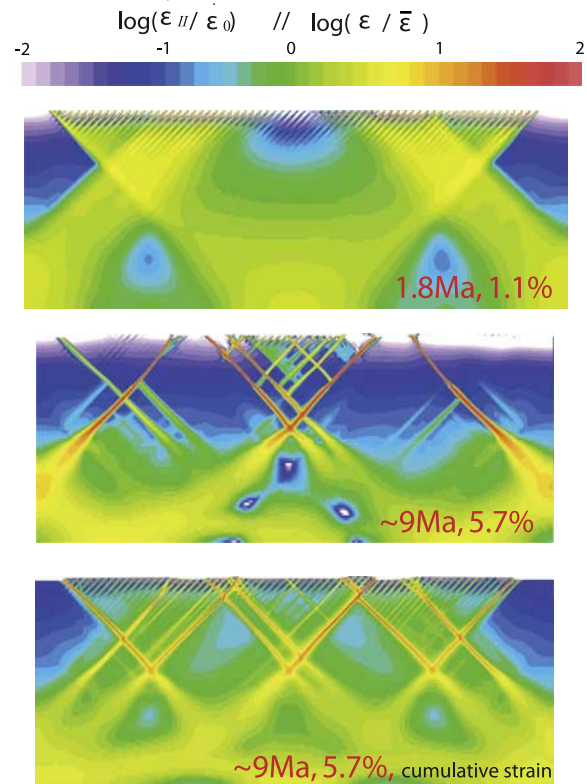


**Figure 4.** Numerical model of selective abandonment. (top) Strain-rate after 1.8 Ma of shortening: the entire preexisting fabric has been reactivated, and abandonment is about to start. (middle) Strain-rate after 9 Ma: strain-rate is maximum along localized widely-spaced shear bands, with residual activity along the preexisting fabric. (bottom) Cumulative strain at the end of the run, showing a fault pattern similar to the Central Indian Basin (see auxiliary material Text S1 and Figure S1).

<sup>1</sup>Auxiliary materials are available in the HTML. doi:10.1029/2008GL035066.



~50 m. The resulting shortening is significant since it reaches at least 1%. The final picture is a set of sealed small faults and active large faults.

[19] **Acknowledgments.** We thank Jonathan Bull and Magali Billen for their very constructive reviews. L. G. J. M. was supported by grant OCE-0623188 and a visiting professorship from the Ecole Normale Supérieure.

## References

- Antolik, M., R. E. Abercrombie, J. Pan, and G. Ekström (2006), Rupture characteristics of the 2003  $M_w$  7.6 mid-Indian Ocean earthquake: Implications for seismic properties of young oceanic lithosphere, *J. Geophys. Res.*, *111*, B04302, doi:10.1029/2005JB003785.
- Beeler, N. M., T. E. Tullis, and J. D. Weeks (1996), Frictional behavior of large displacement experimental faults, *J. Geophys. Res.*, *101*, 8697–8715.
- Behn, M. D., J. Lin, and M. T. Zuber (2002), A continuum mechanics model for normal faulting using a strain-rate softening rheology: Implications for thermal and rheological controls on continental and oceanic rifting, *Earth Planet. Sci. Lett.*, *202*, 725–740.
- Billen, M. I., E. Cowgill, and E. Buer (2007), Determination of fault friction from reactivation of abyssal-hill faults in subduction zones, *Geology*, *35*(9), 819–822, doi:10.1130/G23847A.
- Bohnenstiehl, D. R., M. Tolstoy, and E. Chapp (2004), Breaking into the plate: A 7.6 Mw fracture-zone earthquake adjacent to the Central Indian Ridge, *Geophys. Res. Lett.*, *31*, L02615, doi:10.1029/2003GL018981.
- Bull, J. M., and R. A. Scrutton (1990), Fault reactivation in the central Indian Ocean and the rheology of oceanic lithosphere, *Nature*, *344*, 855–858.
- Bull, J. M., and R. A. Scrutton (1992), Seismic reflection images of intraplate deformation, central Indian Ocean, and their tectonic significance, *J. Geol. Soc. London*, *149*, 955–966.
- Chamot-Rooke, N., F. Jestin, and B. De Voogd (1993), Intraplate shortening in the central Indian Ocean determined from a 2100-km-long north-south deep seismic reflection profile, *Geology*, *21*, 1043–1046.
- Chen, Y., and W. J. Morgan (1990), A nonlinear rheology model for mid-ocean ridge axis topography, *J. Geophys. Res.*, *95*, 17,583–17,604.
- Cloetingh, S., and R. Wortel (1986), Stress in the Indo-Australian plate, *Tectonophysics*, *132*, 49–67.
- Cochran, J. R., et al. (1989), Intraplate deformation and Bengal fan sedimentation: Background and objectives, *Proc. Ocean Drill. Program Initial Rep.*, *116*, 3–11.
- Delescluse, M., and N. Chamot-Rooke (2007), Instantaneous deformation and kinematics of the India-Australia plate, *Geophys. J. Int.*, *168*, 818–842.
- Delescluse, M., and N. Chamot-Rooke (2008), Very first pulse of deformation at 9 Ma in the Central Indian Basin, *Geophys. Res. Abstr.*, *10*, 06888.
- DeMets, C., R. G. Gordon, and J. Y. Royer (2005), Motion between the Indian, Capricorn and Somalian plates since 20 Ma: Implications from the timing and magnitude of distributed lithospheric deformation in the equatorial Indian Ocean, *Geophys. J. Int.*, *161*, 445–468.
- Deplus, C., et al. (1998), Direct evidence of active deformation in the eastern Indian oceanic plate, *Geology*, *26*, 131–134.
- Eittreim, S. L., and J. Ewing (1972), Mid-plate tectonics in the Indian Ocean, *J. Geophys. Res.*, *77*, 6413–6421.
- Gerbault, M. (2000), At what stress level is the central Indian Ocean lithosphere buckling?, *Earth Planet. Sci. Lett.*, *178*, 165–181.
- Gordon, R. G. (2000), Diffuse oceanic plate boundaries: Strain rates, vertically averaged rheology, and comparisons with narrow plate boundaries and stable interiors, in *The History and Dynamics of Global Plate Motions*, *Geophys. Monogr. Ser.*, vol. 121, edited by M. A. Richards, R. G. Gordon, and R. D. van der Hilst, pp. 143–159, AGU, Washington, D. C.
- Krishna, K. S., J. M. Bull, and R. A. Scrutton (2001), Evidence for multi-phase folding of the central Indian Ocean lithosphere, *Geology*, *29*, 715–718.
- Marone, C., and S. J. D. Cox (1994), Scaling of rock friction constitutive parameters: The effects of surface roughness and cumulative offset on friction of gabbro, *Pure Appl. Geophys.*, *143*, 359–386.
- Masson, D. G. (1991), Fault patterns at outer trench walls, *Mar. Geophys. Res.*, *13*, 209–225, doi:10.1007/BF00369150.264.
- Montési, L. G. J., and M. T. Zuber (2003a), Spacing of faults at the scale of the lithosphere and localization instability: 2. Application to the Central Indian Basin, *J. Geophys. Res.*, *108*(B2), 2111, doi:10.1029/2002JB001924.
- Montési, L. G. J., and M. T. Zuber (2003b), Clues to the lithospheric structure of Mars from wrinkle ridge sets and localization instability, *J. Geophys. Res.*, *108*(E6), 5048, doi:10.1029/2002JE001974.
- Montési, L. G. J., and M. T. Zuber (2003c), Spacing of faults at the scale of the lithosphere and localization instability: 1. Theory, *J. Geophys. Res.*, *108*(B2), 2110, doi:10.1029/2002JB001923.
- Neumann, G., and M. T. Zuber (1995), A continuum approach to the development of normal faults, in *Rock Mechanics: Proceedings of the 35th U. S. Symposium on Rocks Mechanics*, pp. 191–198, A. A. Balkema, Rotterdam, Netherlands.
- Okal, E. A. (1983), Oceanic intraplate seismicity, *Annu. Rev. Earth Planet. Sci.*, *11*, 195–214.
- Ranero, C. R., J. P. Morgan, K. McIntosh, and C. Reichert (2003), Bending-related faulting and mantle serpentinization at the middle America trench, *Nature*, *425*, 367–373.
- Sandwell, D. T., and W. H. F. Smith (1997), Marine gravity anomaly from Geosat and ERS-1 satellite altimetry, *J. Geophys. Res.*, *102*(B5), 10,039–10,054.
- Tinnon, M. J., W. E. Holt, and A. J. Haines (1995), Velocity gradients in the northern Indian Ocean inferred from earthquake moment tensors and relative plate velocities, *J. Geophys. Res.*, *100*, 24,315–24,329.
- Van Orman, J., J. R. Cochran, J. K. Weissel, and F. Jestin (1995), Distribution of shortening between the Indian and Australian plates in the central Indian Ocean, *Earth Planet. Sci. Lett.*, *133*, 35–46.
- Weissel, J. K., R. N. Anderson, and C. A. Geller (1980), Deformation of the Indo-Australian plate, *Nature*, *287*, 284–291.

N. Chamot-Rooke and M. Delescluse, Laboratoire de Géologie, Ecole Normale Supérieure, CNRS, 24 rue Lhomond, F-75005 Paris, France. (delesclu@geologie.ens.fr)

L. G. J. Montési, Department of Geology, University of Maryland, College Park, MD 20782, USA.